

RESEARCH ARTICLE

10.1002/2014JA020918

Key Points:

- Electrons can be accelerated in the DF by a betatron process
- Electrons can be trapped in the electric potential and get accelerated
- There is a velocity threshold below which the electrons can be energized

Correspondence to:

Q. Lu,
qmlu@ustc.edu.cn

Citation:

Huang, C., M. Wu, Q. Lu, R. Wang, and S. Wang (2015), Electron acceleration in the dipolarization front driven by magnetic reconnection, *J. Geophys. Res. Space Physics*, 120, 1759–1765, doi:10.1002/2014JA020918.

Received 4 DEC 2014

Accepted 10 FEB 2015

Accepted article online 15 FEB 2015

Published online 14 MAR 2015

Electron acceleration in the dipolarization front driven by magnetic reconnection

Can Huang^{1,2}, Mingyu Wu¹, Quanming Lu^{1,2}, Rongsheng Wang³, and Shui Wang¹

¹CAS Key Laboratory of Geospace Environment, Department of Geophysics and Planetary Science, University of Science and Technology of China, Hefei, China, ²Collaborative Innovation Center of Astronautical Science and Technology, Harbin, China, ³Key Laboratory of Ionospheric Environment, Institute of Geology and Geophysics, Chinese Academy of Sciences, Beijing, China

Abstract A large-scale two-dimensional (2-D) particle-in-cell simulation is performed in this paper to investigate electron acceleration in the dipolarization front (DF) region during magnetic reconnection. It is found that the DF is mainly driven by an ion outflow which also generates a positive potential region behind the DF. The DF propagates with an almost constant speed and gets growing, while the electrons in the DF region can be highly energized in the perpendicular direction due to betatron acceleration. For the first time, we reveal that there exists a velocity threshold; only the electrons below the threshold can be trapped by the parallel electric potential in the DF region and then energized by betatron acceleration.

1. Introduction

Magnetic reconnection is often involved to explain plasma heating and acceleration with a sudden release of magnetic free energy [Vasyliunas, 1975; Biskamp, 2000; Priest and Forbes, 2000] in plasmas ranging from solar atmosphere [Giovanelli, 1946; Masuda et al., 1994] to the planet's magnetosphere [Øieroset et al., 2002; Wang et al., 2010; Zhang et al., 2012] and laboratory experiments [Ji et al., 1998; Li et al., 2007; Dong et al., 2012]. Magnetic reconnection also significantly affects the downstream signatures such as the dipolarization front (DF) [Angelopoulos et al., 1992; Fu et al., 2013] and the energetic electrons [Vaivads et al., 2011].

The DF usually emerges in the reconnection jet and is regarded as the leading edge of the propagating magnetic flux pileup region [Nakamura et al., 2002; Runov et al., 2009]. As a boundary with a typical scale of about one ion inertial lengths, the DF is a nature separator between the hot and tenuous plasma and the ambient cold and dense plasma sheet [Runov et al., 2011]. Earlier magnetohydrodynamic simulations [e.g., Hesse and Birn, 1994] and hybrid simulations of magnetic reconnection [e.g., Hesse et al., 1998] found a sharp enhancement of B_z normal to the neutral plane in the outflow region (which can be regarded as a DF), and it propagates earthward in the magnetotail. From a theoretical point, a DF can be considered as a generic and transient signature associated with reconnection rather than a consequence of the compression of the Earth's intrinsic magnetic field. Recently, Sitnov et al. [2009] use particle-in-cell (PIC) simulations with open boundary conditions to investigate the propagation of the DFs driven by a transient magnetic reconnection. Their results are in agreement with the observation of Runov et al. [2009].

The production of energetic electrons is one of the important signatures in magnetic reconnection. In the diffusion region, electrons can be accelerated by a multistep process [Hoshino et al., 2001; Huang et al., 2010]. Magnetic island is also thought as an accelerator for electrons, which can gain kinetic energy by reflecting from the ends of the contracting magnetic islands [Fu et al., 2006; Drake et al., 2006]. Using the satellite data, Imada et al. [2007] found that energetic electrons can be produced by a nonadiabatic process in the pileup region, which is between the X line and the DF. Recently, satellite observations in the Earth's magnetotail have revealed that the enhancement of energetic electrons associated with DFs, and an adiabatic process, such as betatron or Fermi acceleration, is considered to be the dominant mechanism to energize electrons [Smets et al., 1999; Birn et al., 2004; Wu et al., 2006; Ashour-Abdalla et al., 2011; Fu et al., 2013]. The acceleration in the DF region is regarded as an important ingredient to electron energization during magnetic reconnection [Fu et al., 2013; Wu et al., 2013]. In the Earth's magnetosphere, DFs are also suggested to be associated with aurorae and substorms [Baumjohann et al., 1999; Volwerk et al., 2008]. They usually move near the leading edge of flow bursts inside bursty bulk flows [Birn et al., 2004;

Ashour-Abdalla et al., 2011], which dominate the transport of plasma and magnetic flux in the magnetotail [Angelopoulos et al., 1992; Slavin et al., 2003; Ohtani et al., 2004].

However, until now, little is known about the microscopic mechanism of the adiabatic electron acceleration in a DF driven by magnetic reconnection. In this paper, with a large-scale two-dimensional (2-D) PIC simulation, we find that electron acceleration in a DF region is attributed to a betatron acceleration process, where a trapping mechanism due to the parallel electric potential is revealed for the first time to play an essential role. Only the electrons with smaller parallel velocity can be trapped and suffer betatron acceleration, which results in a pancake distribution.

2. Simulation Model

An initial Harris current sheet equilibrium with a particle number density $n(z) = n_b + n_0 \operatorname{sech}^2(z/\delta)$ is used in the simulation, where $n_b = 0.1 n_0$ represents the background density and $\delta = 0.5 c/\omega_{pi}$ is the half width of the current sheet (c/ω_{pi} is the ion inertial length). The corresponding magnetic field is given by $B(z) = B_0 \tanh(z/\delta) \mathbf{e}_x$, where B_0 is the asymptotical magnetic field. All of the particles are assumed to satisfy the Maxwellian distribution, with an initial temperature ratio $T_{i0}/T_{e0} = 5$. The rest mass ratio is set to be $m_i/m_e = 25$, where the subscripts i and e stand for ion and electron, respectively. The light speed is assumed to be $c = 15V_A$, where V_A is the Alfvén speed based on B_0 and n_0 . The unrealistic mass ratio and light speed are used here because of the limited computing power. Previous researches have shown that the change of the mass ratio and the light speed have little effects on the reconnection rate, the structures of the electromagnetic field, and the evolution of magnetic reconnection [Pritchett, 2001; Fujimoto, 2006; Guo and Lu, 2007]. We can expect that the used unrealistic mass ratio and light speed will not change the process of electron acceleration studied in this paper. In PIC simulations, the electromagnetic fields are defined on the grids and updated by integrating the Maxwell equations with an explicit leapfrog scheme, while the ions and electrons are treated as individual particles and advanced in these electromagnetic fields. The simulation is performed in the (x, z) plane, and a large-scale computational domain size $L_x \times L_z = 204.8c/\omega_{pi} \times 25.6c/\omega_{pi}$ is used here with the spatial resolution $\Delta x = \Delta z = 0.05c/\omega_{pi}$. The time step is set to be $\Delta t = 0.001\Omega_i^{-1}$, where $\Omega_i = eB_0/m_i$ is the ion gyrofrequency in the asymptotical magnetic field. More than 10^9 particles every species are employed in the simulation. Periodic boundary conditions are assumed in the x direction, while in the z direction, conducting boundary conditions are retained and particles are specularly reflected. The reconnection is initiated by a small flux perturbation.

3. Simulation Results

In the simulation, magnetic reconnection occurs around $\Omega_i t = 10$, and only a single X point appears around $x = 102c/\omega_{pi}$ in the long current sheet, which allows us to trace the DF before the computational boundary can influence the structure of this DF. In order to investigate the generation of the DF in magnetic reconnection, in Figure 1, we plot the time evolutions of (a) B_z , (b) $\partial V_{ix}/\partial x$, (c) $(\nabla \times \mathbf{R}_e)_z$, (d) $-B_z \partial V_{ex}/\partial x$, (e) $(\nabla \times \mathbf{R}_i)_z$, and (f) $-B_z \partial V_{ix}/\partial x$ along $z = 0$ during the time interval $15 \leq \Omega_i t \leq 35$. Here B_z presents the magnitude of the DF and $\mathbf{R}_{i,e} = \mathbf{E} + \mathbf{V}_{i,e} \times \mathbf{B}$ is the nonideal electric field in the ion/electron frame. The white dotted and solid lines denote $\Omega_i t = 19$ and 22, respectively. The silver curves represent the contours of the in-plane magnetic flux for reference. The magnitude of B_z increased at about $\Omega_i t = 15$, and a DF is then formed. At the same time, the DF propagates away from the X line with a constant speed of about V_A . Figures 1c and 1e show that $(\nabla \times \mathbf{R}_e)_z$ and $(\nabla \times \mathbf{R}_i)_z$ stay almost zero at $\Omega_i t \approx 19$ and 22, respectively, meaning that electrons and ions are frozen with the magnetic field from these corresponding times. According to Faraday's law $\partial \mathbf{B}/\partial t = \nabla \times \mathbf{E}$, after assuming $\partial/\partial y = 0$ and $B_x = B_y = 0$ along $z = 0$ (B_x and B_y are much smaller than B_z in the midplane), we can find that the evolution of B_z along $z = 0$ can be described by $DB_z/Dt = -B_z \partial V_{sx}/\partial x$ when $(\nabla \times \mathbf{R}_s)_z = 0$ (here D/Dt is the material derivative in the fluid frame and $s = i, e$ represent ions and electrons, respectively). Therefore, from Figures 1d and 1f, we can know that the pileup of the magnetic field in the DF region is driven mainly by the electron flow between about $\Omega_i t = 19$ and 22 and by the ion flow from about $\Omega_i t = 22$.

Electrons are found to be obviously accelerated in the DF region when the growing DF is propagating away from the diffusion region, and the details are described in Figure 2. Figure 2a shows the spatial distribution

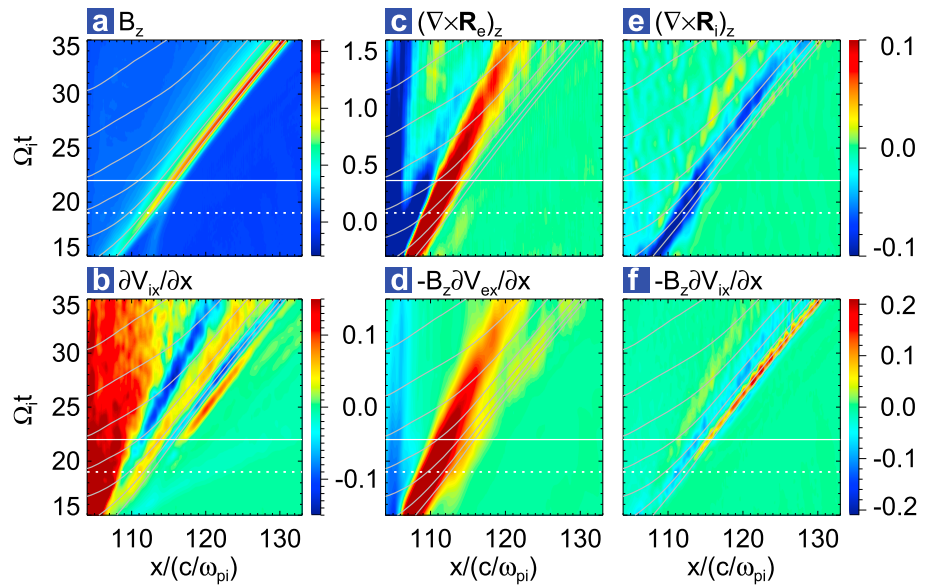


Figure 1. The time evolutions of (a) B_z , (b) $\partial V_{ix}/\partial x$, (c) $(\nabla \times \mathbf{R}_e)_z$, (d) $-B_z \partial V_{ex}/\partial x$, (e) $(\nabla \times \mathbf{R}_i)_z$, and (f) $-B_z \partial V_{ix}/\partial x$ along $z=0$ from $\Omega_i t=15$ to 35. The white dotted and solid lines denote $\Omega_i t=19$ and 22, respectively. The silver curves represent the contours of the in-plane magnetic flux for reference.

of the energy flux $\int_{\varepsilon_0}^{\infty} \varepsilon f(\varepsilon) d\varepsilon$ (where $\varepsilon_0=0.1 m_e c^2$) of the energetic electrons at $\Omega_i t=35$. Here the electron kinetic energy is calculated by $\varepsilon=(\gamma-1)m_e c^2$, where γ is the relativity factor. Figure 2b describes the electron distribution $f(v_{e\parallel}, v_{e\perp})$ in the DF region, while Figure 2c plots the energy spectrum of the energetic electrons in the DF region at $\Omega_i t=25$ (blue) and 35 (red). As reported in the previous studies [Imada et al., 2007], electrons can be accelerated in the vicinity of the X line and the magnetic field pileup region with the obvious

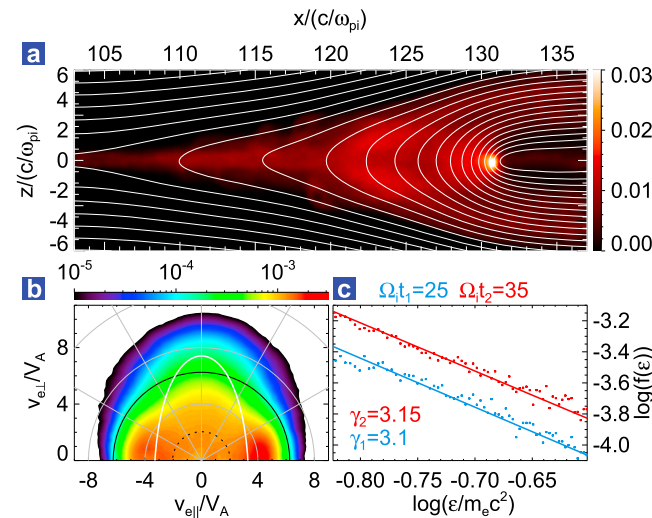


Figure 2. (a) The energy flux of electrons whose kinetic energy is greater than $0.1m_e c^2$ ($\int_{0.1m_e c^2}^{\infty} \varepsilon f(\varepsilon) d\varepsilon$), (b) the velocity space distribution of electrons $f(v_{e\parallel}, v_{e\perp})$ in the vicinity of the DF ($130 \leq x/(c/\omega_{pi}) \leq 131$, $-0.5 \leq z/(c/\omega_{pi}) \leq 0.5$) at $\Omega_i t=35$, and (c) the electron energy spectrum in the vicinity of the DF at $\Omega_i t=25$ (blue) and 35 (red). The power law curves are fitted as $\propto \varepsilon^{-\gamma}$ with energy range from $0.15m_e c^2$ to $0.25m_e c^2$. The white contours in Figure 2a represent the in-plane magnetic field lines. The dotted and black semicircles in Figure 2b denote the initial thermal velocity and $\varepsilon=0.1 m_e c^2$, respectively. The white curve denotes the velocity threshold mentioned in the following text.

enhancement of the electron flux. In this paper, we find that the electron energy flux can be further enhanced in the DF region. In the DF region, the electrons show a pancake distribution (the pitch angles are concentrated around 90°) in the higher-energy range ($v_e > 6 V_A$) and a cigar distribution (the pitch angles are concentrated around 0° and 180°) in the lower-energy range ($2 V_A < v_e < 5 V_A$). From Figure 2c, we can also find that the electron energy spectrum in the DF region has a power law distribution at higher-energy range, and the index of the spectrum is almost kept as a constant (around 3.1) during its propagation, which means that the acceleration of the energetic electrons associated with the DF may be an adiabatic process.

The formation of the significant electron energy flux in the DF region can be explained by tracing the energetic electrons, which are shown in Figure 3. Figure 3 plots the positions of the

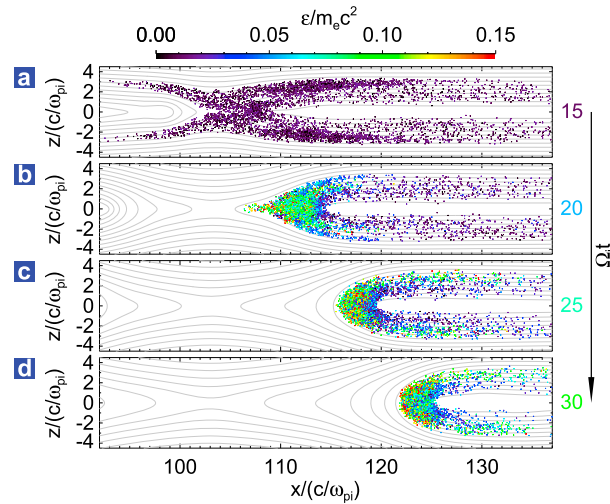


Figure 3. The positions of the electrons that suffered acceleration near the DF at (a) $\Omega_i t = 15$, (b) 20, (c) 25, and (d) 30. The kinetic energies of these traced electrons are greater than $0.1 m_e c^2$ at $\Omega_i t = 35$ in the vicinity of the DF. The colors of the dots present the kinetic energies for each electron, and the colors of the figures on the right side denote the mean kinetic energies of these electrons at different times. The silver contours represent the in-plane magnetic field lines.

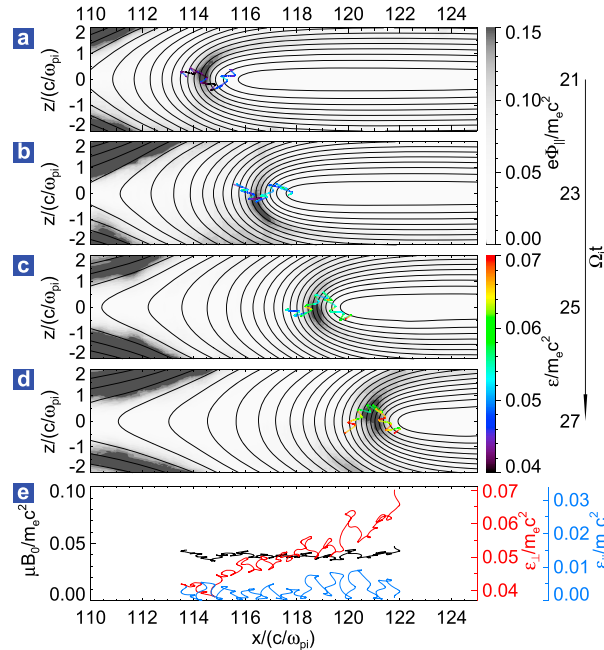


Figure 4. (a–d) The trajectories of the most energetic electron during (a) $20.1 \leq \Omega_i t \leq 22$, (b) $22 \leq \Omega_i t \leq 24$, (c) $24 \leq \Omega_i t \leq 26$, and (d) $26 \leq \Omega_i t \leq 27.8$. The colors of the trajectory indicate the kinetic energies, while the background images are the parallel electric potential at $\Omega_i t = 21, 23, 25$, and 27 . (e) The whole trajectory is shown in a format of electron magnetic moment $\mu B_0 / m_e c^2$ (black), perpendicular kinetic energy $\epsilon_{\perp} / m_e c^2$ (red), and parallel kinetic energy $\epsilon_{\parallel} / m_e c^2$ (blue) versus the spatial location x . The black solid contours represent the in-plane magnetic field lines.

electrons that suffered from the acceleration associated with the DF at different times. These electrons are chosen in the vicinity of the DF (a $c/\omega_{pi} \times c/\omega_{pi}$ box around the B_z peak) at $\Omega_i t = 35$, with the kinetic energies greater than $0.1 m_e c^2$. The colors of the figures on the right side denote the mean kinetic energies of these electrons at different times. Most electrons are trapped near the DF. They move away from the diffusion region and get accelerated in the growing DF. Such image indicates that the energy flux enhancement in Figure 2a is not attributed to the transport effect but the local acceleration.

In order to clarify the acceleration mechanism, the illustrations for some typical electron trajectories are necessary. Figures 4a–4d show the trajectory of the most energetic electron during different time intervals, while Figures 5a–5d plot the trajectory of the electron that suffered insignificant acceleration. Figures 4e and 5e describe the magnetic momentum $\mu B_0 / m_e c^2$ (black), perpendicular kinetic energy $\epsilon_{\perp} / m_e c^2$ (red), and parallel kinetic energy $\epsilon_{\parallel} / m_e c^2$ versus its position x for the most energetic electron and the electron that suffered insignificant acceleration, respectively. In the figure, the colors of the trajectories indicate the kinetic energies, and the background images show the parallel electric potential, which is defined by $\Phi_{\parallel}(\mathbf{r}) = \int_{\mathbf{r}} E_{\parallel} ds$ (the line integral is along the magnetic field lines) as in Egedal *et al.* [2008]. The magnetic field lines are also plotted for reference. We can find that the magnetic moment of both the electrons are almost kept as constant. For the most energetic electron, its parallel velocity is small when it enters the DF region; therefore, the electron can be trapped by the electric potential for longer time and accelerated to the higher energy in the perpendicular direction by the inductive electric field. The inductive electric field in the DF region is generated due to the increase of B_z during the propagation and compression of the DF. Therefore, the electron is energized by betatron acceleration, and this kind of electrons with higher energy forms a pancake distribution. The electron, which suffered insignificant acceleration, has a

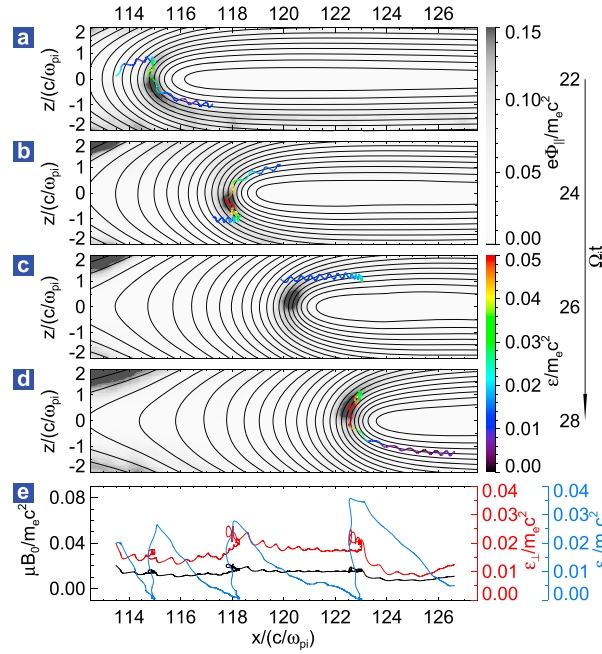


Figure 5. Same format as Figure 4. (a–d) The trajectory of the electron that suffered insignificant acceleration during (a) $20.05 \leq \Omega_e t \leq 22.5$, (b) $22.5 \leq \Omega_e t \leq 24.5$, (c) $24.5 \leq \Omega_e t \leq 27.5$, and (d) $27.5 \leq \Omega_e t \leq 30$. The parallel electric potentials are obtained at $\Omega_e t = 22, 24, 26$, and 28 .

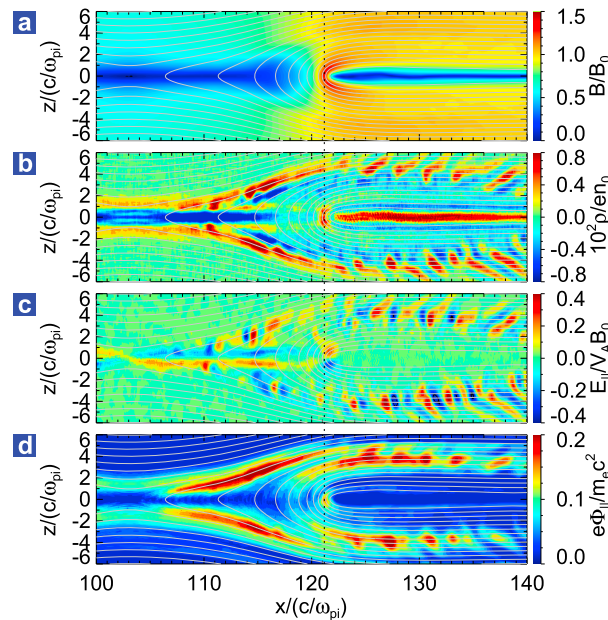


Figure 6. (a) The intensity of the magnetic field B/B_0 , (b) charge density $10^2 \rho/en_0$, (c) parallel electric field $E_{||}/V_A B_0$, and (d) parallel electric potential $e\Phi_{||}/m_e c^2$ at $\Omega_e t = 26.8$. The silver contours represent the in-plane magnetic field lines, while the dotted line denotes the position of the DF in the x direction.

larger parallel velocity when it goes into the DF region. Therefore, the electron can move through the DF region quickly and cannot be accelerated to a high energy. Such kind of electrons forms a cigar distribution. So it is easy to understand the causes of the electron distribution in Figure 2b.

The parallel electric field in the DF region plays an important role during betatron acceleration of the electrons, and its generation can be understood in Figure 6, which plots (a) the intensity of the magnetic field B/B_0 , (b) the charge density $10^2 \rho/en_0$, (c) the parallel electric field $E_{||}/V_A B_0$, and (d) the parallel electric potential $e\Phi_{||}/m_e c^2$ at $\Omega_e t = 26.8$. The dotted line denotes the position of the DF in the x direction. The magnetic field is greatly enhanced in the DF region. The ion bulk flow is then decelerated in this region (see Figure 1b), which leads to the accumulation of the ions and a positive charge density. Then, a parallel electric field with a positive parallel electric potential is generated in the DF region.

Therefore, the electron behavior in the DF region is determined by two forces: the “pushing” force $F_{\text{mirror}} = -\mu \partial B / \partial s$ (where s is the position vector measured along the magnetic field line) and the “pulling” force $F_{E_{||}} = -eE_{||}$. After integrating the work done by the two forces along the magnetic field line, we can obtain $\epsilon_{||}(\mathbf{r}_2) = \epsilon_{||}(\mathbf{r}_1)$

$$-\int_{\mathbf{r}_1}^{\mathbf{r}_2} (\mu \partial B / \partial s + eE_{||}) ds.$$
 After we set $\epsilon_{||\text{Edge}} = 0$ ($\epsilon_{||\text{Edge}}$ is the parallel kinetic energy at the edge of the DF region), a velocity threshold, where electrons are trapped within the DF region and then get accelerated, can be expressed as $\frac{v_{||}^2}{\gamma+1}$

$$\left[\left(\frac{v_{||}}{c} \right)^2 + \left(1 - \frac{B_{\text{Edge}}}{B_{\text{DF}}} \right) \left(\frac{v_{\perp}}{c} \right)^2 \right] = \frac{e(\Phi_{||\text{DF}} - \Phi_{||\text{Edge}})}{m_e c^2}$$
 (where $\Phi_{||\text{Edge}}$ and B_{Edge} are the potential and magnetic field at the edge of the DF region, while $\Phi_{||\text{DF}}$ and B_{DF} are the parallel electric potential and magnetic field at the center of DF region). Therefore, only the electrons below the threshold can be trapped in the DF region and suffer obvious betatron acceleration. The potential difference $e(\Phi_{||\text{DF}} - \Phi_{||\text{Edge}})/m_e c^2$ and the magnetic field ratio $B_{\text{Edge}}/B_{\text{DF}}$ can be estimated to about 0.1 and 0.8 during the

time interval $25 \leq \Omega_e t \leq 35$, and the threshold can be easily obtained, which is plotted in Figure 2b with the white curve. The electrons within the white curve are energized in the perpendicular direction and present a pancake distribution at last, while other electrons form a cigar distribution. Our simulation results (shown in Figure 2b) are consistent with the theoretical prediction.

4. Summary

In this paper, with a large-scale 2-D PIC simulation, we investigate the mechanism of electron acceleration in the DF region of magnetic reconnection. The DF is found to be driven first by an electron outflow and then by an ion flow. Electrons in the DF region can be accelerated by a betatron acceleration process. For the first time, we find the existence of a velocity threshold, which is related to the trapping mechanism due to the parallel electric potential in the DF region. The threshold categorizes the electrons into two types. Only the electrons below the threshold can be accelerated in the perpendicular direction by betatron acceleration. These electrons form a pancake distribution, which has been observed by satellite in the DF region [e.g., Wu *et al.*, 2013]. The parallel electric potential in the DF region plays an important role on the electron trapping. It is caused by the charge separation between electrons and ions. When the mass ratio is sufficiently large, such effects will become more significant with the increase of the mass ratio.

Acknowledgments

This research was supported by the National Science Foundation of China grants 41331067, 11220101002, 41204103, and 11235009; 973 Program (2013CBA01503 and 2012CB825602); and the Specialized Research Fund for State Key Laboratories, CAS Key Research Program KZZD-EW-01-4. The results are generated from our computer simulation code as described in section 2. The data can be obtained by contacting the corresponding author through e-mail (qmlu@ustc.edu.cn).

Michael Liemohn thanks Enrico Camporeale and another reviewer for their assistance in evaluating this paper.

References

- Angelopoulos, V., W. Baumjohann, C. F. Kennel, F. V. Coroniti, M. G. Kivelson, R. Pellat, R. J. Walker, H. Lüher, and G. Paschmann (1992), Bursty bulk flows in the inner central plasma sheet, *J. Geophys. Res.*, *97*, 4027–4039, doi:10.1029/91JA02701.
- Ashour-Abdalla, M., M. El-Alaoui, M. L. Goldstein, M. Zhou, D. Schriver, R. Richard, R. Walker, M. G. Kivelson, and K. Hwang (2011), Observations and simulations of nonlocal acceleration of electrons in magnetotail magnetic reconnection events, *Nat. Phys.*, *7*, 360–365, doi:10.1038/nphys1903.
- Baumjohann, W., M. Hesse, S. Kokubun, T. Mukai, T. Nagai, and A. A. Petrukovich (1999), Substorm dipolarization and recovery, *J. Geophys. Res.*, *104*, 24,995–25,000, doi:10.1029/1999JA900282.
- Birn, J., M. F. Thomsen, and M. Hesse (2004), Electron acceleration in the dynamic magnetotail: Test particle orbits in three-dimensional magnetohydrodynamic simulation fields, *Phys. Plasmas*, *11*, 1825–1833, doi:10.1063/1.1704641.
- Biskamp, D. (2000), *Magnetic Reconnection in Plasmas*, p. 3, Cambridge Univ. Press, Cambridge, U. K.
- Dong, Q. L., et al. (2012), Plasmoid ejection and secondary current sheet generation from magnetic reconnection in laser-plasma interaction, *Phys. Rev. Lett.*, *108*, 215,001, doi:10.1103/PhysRevLett.108.215001.
- Drake, J. F., M. Swisdak, H. Che, and M. A. Shay (2006), Electron acceleration from contracting magnetic islands during reconnection, *Nature*, *443*, 553–556, doi:10.1038/nature05116.
- Egedal, J., W. Fox, N. Katz, M. Porkolab, M. Øieroset, R. P. Lin, W. Daughton, and J. F. Drake (2008), Evidence and theory for trapped electrons in guide field magnetotail reconnection, *J. Geophys. Res.*, *113*, A12207, doi:10.1029/2008JA013520.
- Fu, H. S., Y. V. Khotyaintsev, A. Vaivads, A. Retinò, and M. André (2013), Energetic electron acceleration by unsteady magnetic reconnection, *Nat. Phys.*, *9*, 426–430, doi:10.1038/nphys2664.
- Fu, X. R., Q. M. Lu, and S. Wang (2006), The process of electron acceleration during collisionless magnetic reconnection, *Phys. Plasmas*, *13*, 012,309.
- Fujimoto, K. (2006), Time evolution of the electron diffusion region and the reconnection rate in fully kinetic and large system, *Phys. Plasmas*, *13*, 072904, doi:10.1063/1.2220534.
- Giovanelli, R. G. (1946), A theory of chromospheric flares, *Nature*, *158*, 81, doi:10.1038/158081a0.
- Guo, J., and Q. M. Lu (2007), Effects of ion to electron mass ratio on electron dynamics in collisionless magnetic reconnection, *Chin. Phys. Lett.*, *24*, 3199–3202.
- Hesse, M., and J. Birn (1994), MHD modeling of magnetotail instability for localized resistivity, *J. Geophys. Res.*, *99*, 8565–8576, doi:10.1029/94JA00441.
- Hesse, M., J. Birn, and D. Winske (1998), Formation and structure of thin current sheets in the magnetotail: Dipolarization, in *Substorms 4*, edited by S. Kokubun and Y. Kamide, pp. 727–730, Kluwer Acad., Boston, Mass.
- Hoshino, M., T. Mukai, T. Terasawa, and I. Shinohara (2001), Suprathermal electron acceleration in magnetic reconnection, *J. Geophys. Res.*, *106*, 25,979–25,997, doi:10.1029/2001JA900052.
- Huang, C., Q. M. Lu, and S. Wang (2010), The mechanisms of electron acceleration in antiparallel and guide field magnetic reconnection, *Phys. Plasmas*, *17*, 072,306, doi:10.1063/1.3457930.
- Imada, S., R. Nakamura, P. W. Daly, M. Hoshino, W. Baumjohann, S. Mühlbacher, A. Balogh, and H. Rème (2007), Energetic electron acceleration in the downstream reconnection outflow region, *J. Geophys. Res.*, *112*, A03202, doi:10.1029/2006JA011847.
- Ji, H. T., M. Yamada, S. Hsu, and R. Kulsrud (1998), Experimental test of the Sweet-Parker model of magnetic reconnection, *Phys. Rev. Lett.*, *80*, 3256–3259, doi:10.1103/PhysRevLett.80.3256.
- Li, C. K., F. H. Séguin, J. A. Frenje, J. R. Rygg, R. D. Petrasso, R. P. Town, O. L. Landen, J. P. Knauer, and V. A. Smalyuk (2007), Observation of Megagauss-field topology changes due to magnetic reconnection in laser-produced plasmas, *Phys. Rev. Lett.*, *99*, 055001, doi:10.1103/PhysRevLett.99.055001.
- Masuda, S., T. Kosugi, H. Hara, S. Tsuneta, and Y. Ogawara (1994), A loop top hard X-ray in a compact solar flare as evidence for magnetic reconnection, *Nature*, *371*, 495–497, doi:10.1038/371495a0.
- Nakamura, R., et al. (2002), Motion of the dipolarization front during a flow burst event observed by Cluster, *Geophys. Res. Lett.*, *29*(20), 1942, doi:10.1029/2002GL015763.
- Ohtani, S. I., M. A. Shay, and T. Mukai (2004), Temporal structure of the fast convective flow in the plasma sheet: Comparison between observations and two-fluid simulations, *J. Geophys. Res.*, *109*, A03210, doi:10.1029/2003JA010002.

- Øieroset, M., R. Lin, and T. Phan (2002), Evidence for electron acceleration up to ~300 keV in the magnetic reconnection diffusion region of Earth's magnetotail, *Phys. Rev. Lett.*, *89*, 195001, doi:10.1103/PhysRevLett.89.195001.
- Priest, E., and T. Forbes (2000), *Magnetic Reconnection: MHD Theory and Applications*, p. 6, Cambridge Univ. Press, Cambridge, U. K.
- Pritchett, P. L. (2001), Geospace Environment Modeling magnetic reconnection challenge: Simulations with a full particle electromagnetic code, *J. Geophys. Res.*, *106*(A3), 3783–3798, doi:10.1029/1999JA001006.
- Runov, A. V., V. Angelopoulos, M. I. Sitnov, V. A. Sergeev, J. Bonnell, J. P. McFadden, D. Larson, K.-H. Glassmeier, and U. Auster (2009), THEMIS observations of an earthward propagating dipolarization front, *Geophys. Res. Lett.*, *36*, L14106, doi:10.1029/2009GL038980.
- Runov, A., V. Angelopoulos, X.-Z. Zhou, X.-J. Zhang, S. Li, F. Plaschke, and J. Bonnell (2011), A THEMIS multicase study of dipolarization fronts in the magnetotail plasma sheet, *J. Geophys. Res.*, *116*, A05216, doi:10.1029/2010JA016316.
- Sitnov, M. I., M. Swisdak, and A. V. Divin (2009), Dipolarization fronts as a signature of transient reconnection in the magnetotail, *J. Geophys. Res.*, *114*, A04202, doi:10.1029/2008JA013980.
- Slavin, J. A., et al. (2003), Geotail observations of magnetic flux ropes in the plasma sheet, *J. Geophys. Res.*, *108*(A1), 1015, doi:10.1029/2002JA009557.
- Smets, R., D. Delcourt, J. A. Sauvaud, and P. Koperski (1999), Electron pitch angle distributions following the dipolarization phase of a substorm: Interball-Tail observations and modeling, *J. Geophys. Res.*, *104*, 14,571–14,581, doi:10.1029/1998JA900162.
- Vaivads, A., A. Retino, Y. V. Khotyaintsev, and M. Andre (2011), Suprathermal electron acceleration during reconnection onset in the magnetotail, *Ann. Geophys.*, *29*, 1917–1925, doi:10.5194/angeo-29-1917-2011.
- Vasyliunas, V. M. (1975), Theoretical models of magnetic field line merging, *Rev. Geophys. Space Phys.*, *13*, 303–336, doi:10.1029/RG013i001p00303.
- Volwerk, M., et al. (2008), Magnetotail dipolarization and associated current systems observed by Cluster and Double Star, *J. Geophys. Res.*, *113*, A08S90, doi:10.1029/2007JA012729.
- Wang, R. S., Q. Lu, A. Du, and S. Wang (2010), In situ observations of a secondary magnetic island in an ion diffusion region and associated energetic electrons, *Phys. Rev. Lett.*, *104*, 175003, doi:10.1103/PhysRevLett.104.175003.
- Wu, M. Y., Q. M. Lu, M. Volwerk, Z. Vörös, T. L. Zhang, L. C. Shan, and C. Huang (2013), A statistical study of electron acceleration behind the dipolarization fronts in the magnetotail, *J. Geophys. Res. Space Physics*, *118*, 4804–4810, doi:10.1002/jgra.50456.
- Wu, P., T. A. Fritz, B. Larvaud, and E. Lucek (2006), Substorm-associated magnetotail energetic electrons pitch angle evolutions and flow reversals: Cluster observation, *Geophys. Res. Lett.*, *33*, L17101, doi:10.1029/2006GL026595.
- Zhang, T. L., et al. (2012), Magnetic reconnection in the near Venusian magnetotail, *Science*, *336*, 567–570, doi:10.1126/science.1217013.